Renewable Energy 200 (2022) 492–504

Contents lists available at ScienceDirect

Renewable Energy

journal homepage: www.elsevier.com/locate/renene

Design limits for wave energy converters based on the relationship of power and volume obtained through multi-objective optimisation

Anna Garcia-Teruel [a,*,1], Owain Roberts [b], Donald R. Noble [a], Jillian Catherine Henderson [b], Henry Jeffrey [a]

[a] Institute for Energy Systems, School of Engineering, The University of Edinburgh, Edinburgh, EH9 3DW, United Kingdom
[b] Wave Energy Scotland, An Lòchran, 10 Inverness Campus, Inverness, IV2 5NA, United Kingdom

ARTICLE INFO

Keywords:
Wave energy converter
Design limits
Fundamental relationships
Scale
Size
Capture width

ABSTRACT

Wave energy conversion can have a significant role in the transition to a net-zero energy system. However, cost reductions are still required for this technology to be commercially competitive. To achieve commercialisation at a reasonable expense, disruptive innovations at early stages of development need to be enabled. Thus, to explore more of the design space, design limits need to be defined. Although physical limits, such as the maximum capture width and the Budal upper bound, have been defined, more realistic limits considering the variability of the resource, device dimensions and the actual hydrodynamic behaviour of different shapes can help provide further insights. This is relevant to both technology developers and funding bodies wanting to identify potential areas for innovation. In this study, the use of multi-objective optimisation is proposed to explore these limits, by investigating the optimal relationship between average annual power production and device size. This relationship depends on resource level, mode of motion used for power extraction and hull shape. The obtained fundamental relationships fall within the existing physical limits, but provide further insights into the impact of different factors on these limits. This allows for a more direct comparison with the performance of state-of-the-art wave energy converters.

1. Introduction

Harnessing renewable energy from the waves could provide a significant contribution to future electricity generation. Many wave energy converter (WEC) concepts have been developed and tested over the years, however the levelised cost of energy (LCOE) is still high compared to conventional energy generating technologies. Some previous initiatives have focused on the development and demonstration of existing technologies [1]. Simultaneously, supporting the initial innovation phase of concept creation through structured innovation approaches has proved successful in other sectors [2], but also in the marine energy sector [3]. Recently, enabling disruptive innovations at early stages of development was found to be key to achieve commercialisation at a reasonable public expense [4]. This type of disruptive innovation has been supported, for example, through stage-gated pre-commercial procurement funding programmes such as Wave Energy Scotland's programme [5] and the Wave Energy Prize organised by the United States Department of Energy [6].

1.1. Background

To explore more of the design space and be able to identify potential disruptive solutions, design limits need to be defined. We refer to these limits, as *fundamental relationships*, which are the engineering, physics and underlying economic relationships which drive the earliest stages of assessing the attractiveness of concepts.

To date, a number of physical limits for wave energy conversion have been discussed and are widely used to delimit the physically possible power absorption [7]. The maximum power absorbed by an axisymmetric body based on the power available in the sea is delimited through the maximum Capture Width (CW_{MAX}) definition [8]. This measure reflects the idea that optimal wave energy absorption will occur when the waves generated by the oscillating body result in destructive interference with the incident waves. It describes the maximum power that can be absorbed based on the resource and the radiation pattern, which depends on the mode of oscillation of the device. CW_{MAX} is independent from device features such as geometry or Power Take-Off (PTO) characteristics.

* Corresponding author.
E-mail address: a.garcia-teruel@ed.ac.uk (A. Garcia-Teruel).
[1] Current address: Instituto de Hidráulica Ambiental (IH Cantabria), Parque Científico y Tecnológico de Cantabria, 39011 Santander, Spain.

https://doi.org/10.1016/j.renene.2022.09.053
Received 9 September 2021; Received in revised form 11 August 2022; Accepted 12 September 2022
Available online 19 September 2022

Nomenclature

b	Beam (m)
d	Draft (m)
g	Gravitational acceleration (m/s^2)
r	Radius (m)
w	Width (m)
B	Characteristic width (m)
H_{m0}	Significant wave height (m)
P	Mean produced power per sea state (W)
$\bar{P}$	Mean annual produced power (W)
P_{pm}	Power per metre crest length (W/m)
T_e	Energy period (s)
ρ	Density (kg/m^3)
λ	Wavelength (m)
CW	Capture Width (m)
CW_{MAX}	Maximum Capture Width (m)
CWR	Capture Width Ratio (%)
DoF	Degree of Freedom (NA)
LCOE	Levelised Cost of Energy (NA)
NSGA-II	Non-dominated Sorting Genetic Algorithm II (NA)
PTO	Power Take-Off (NA)
SOTA	State of the Art (NA)
WEC	Wave Energy Converter (NA)

Another physical limit that has been commonly used is the Budal upper bound, which describes the limits of absorbed power for constrained motions in heave for axisymmetric floating bodies with a given submerged volume [9]. This limit definition was extended to consider the absorbed power for stroke constrained motions in multiple modes of motion by Todalshaug [10]. This measure represents the limits of power absorption, considering in addition to resource and radiation pattern, stroke constraints defined through the maximum volume of displaced water. That is, it depends to some extent on the device dimensions.

The theoretical limits for single-degree of freedom WECs were further revisited by Tom in [11] based on a surging only and a heaving only sphere in regular waves. Bounds for the displacement amplitude, time-averaged power and power take-off (PTO) force when applying resistive control were derived.

Similarly, trends for the performance of state-of-the-art wave energy converters were derived by Babarit in [12]. These show how capture width ratio varied with the device's active width based on a thorough review of capture width ratios of different types of devices. These relationships, therefore, represent the WECs state-of-the-art performance depending on device dimension and device type.

For the purpose of identifying areas for potential innovation, the state-of-the-art trends are limited in their ability to explore the design space for solutions that have not yet been invented. This requires going beyond the state of the art and exploring the art of the possible; examining a larger, but still constrained, design space. Simultaneously, existing physical limits may not support the discussion of more specific device design questions, such as: can power performance be improved by adapting the size of the device to a specific location? Or, should different types or shapes of WECs be explored for different types of resource, rather than just varying device sizes?

1.2. Goal

Within the EU H2020 DTOceanPlus project a structured innovation tool was developed to provoke innovation and help represent the voice of the customer through the design process, manage risk and produce new concepts [13]. Alongside this tool, a scenario creation tool was developed in order to guide the creation of new concepts with very minimal inputs. This aims to identify attractive design parameters for potential wave energy converter technologies that have not yet been invented [14]. In both cases, physical wave energy converter design constraints are required to delimit the possible design space, and be able to draw comparison between the 'state of the art' and the 'art of the possible', which is described through these limits. To define these design limits, *fundamental relationships* – describing the relationship between two parameters – can be used. Here, rather than using generic physical constraints such as the maximum capture width or the Budal upper bound, we propose using the results of an optimisation process to find a relationship between average produced power and device dimensions taking into account hull shape and specific resource characteristics. A significant advantage of the approach proposed here is that a number of other different fundamental relationships (e.g. reliability versus average produced power) can be obtained by applying this concept. In this case, the optimisation process is applied to a number of wave energy converter shapes for various locations to define more realistic performance limits, albeit under optimal power absorption conditions. In this way, advantages of more specifically defined devices can be identified in given conditions, and developers may be able to make more direct comparisons based on the found relationships to identify areas for potential innovation.

The paper is organised as follows. In Section 2 the methodology used to generate the more specific performance limits is introduced, and an overview of the considered case studies is provided in Section 2.4. The resulting fundamental relationships are then presented in Section 3 and further discussed in Section 4. Finally, the main conclusions drawn from this study and the scope for future work are outlined in Section 5.

2. Methodology

For the purpose of finding a fundamental relationship between the mean power produced and the dimensions of a wave energy converter, a geometry optimisation tool is applied. The idea behind this is that if optimal geometries for a number of resource conditions are generated, a limit, in terms of how much power can be absorbed for a given device size, will be described by the set of optimal solutions. That is, for a given geometry type and assuming an optimal PTO, the optimisation algorithm will find how much power can be maximally absorbed by a geometry of certain dimensions if the geometry is optimally defined. For the purpose of power absorption, as considered in the Budal upper bound, the submerged volume is a determining factor. This also defines the dimensions of the device. For this reason, in the optimisation process, submerged volume is the metric chosen to represent device size. The wave energy converter geometry optimisation tool was developed and described in detail in [15]. An overview of the optimisation process is provided in Fig. 1 and a summary of the functioning of the tool is provided in the following paragraphs for context. Constraints to the optimisation were purposely defined to allow for a broad search of the optimisation space. Thus, results of the optimisation represent physical limits of what can be achieved under optimal conditions if considering hydrodynamic performance of floating shapes in unidirectional irregular seas.

2.1. Optimisation formulation

Starting from a given geometry definition, a number of geometries of a defined type of wave energy hull (e.g. horizontal cylinder) are randomly generated (see Section 2.2). They are evaluated based on their mean annual power production ($\bar{P}$) to be maximised, and their submerged volume (V) to be minimised. Within an optimisation process, the metrics used to evaluate the best performing solutions are referred

to as objective functions. To calculate the objective function values for each geometry, hydrodynamic characteristics and submerged volume are obtained from the Boundary-Element-Method based software, WAMIT [16]. Regarding the wave climate, different scatter diagrams for different locations are considered, representing low, medium, and high resource locations (see Section 2.3). Irregular seas are considered by using a Bretschneider spectrum. The mean annual power is then calculated for a given location with a pseudo time-domain model [17,18]. That is a frequency-domain model, in which the oscillation time series is evaluated for the purpose of applying stroke constraints in the power production calculation. This means that the method is based on linear wave theory and assumes small oscillations. A semi-optimal impedance matching control is assumed, that considers the wave energy converter is in resonance with the energy period in each sea state. Based on the hydrodynamic modelling approach, this methodology applies to rigid single-body floating devices only.

The optimisation algorithm is then used to select and generate improved shapes, based on the objective function values of each shape. This optimisation process uses a multi-objective meta-heuristic algorithm, the Non-dominated Sorting Genetic Algorithm II (NSGA-II) [19], due to its proven ability to consistently find good solutions to different multi-objective problems. As a genetic algorithm, the NSGA-II emulates evolution theory and the survival of the fittest individuals in a population through selection, crossover and mutation processes. The algorithm implementation builds on [20]. The most suitable genetic operators to be used and the tuning of the optimisation parameters for multi-objective geometry optimisation of WECs using the NSGA-II algorithm was studied in [21]. In that study, crossover and mutation algorithms were compared based on the hypervolume measure. This involved in particular the comparison between using (1) Intermediate Recombination and Breeder Genetic Algorithm Mutation as described in [22], which was previously applied to a similar problem in [23]; and (2) the original formulation by Deb et al. [24,25], which employs a polynomial probability distribution for the crossover and the mutation steps referred to as Simulated Binary Crossover and Polynomial Mutation. The former proved to consistently generate better solutions in all studied cases, and for this reason that implementation is used here. A description of the implemented algorithms based on [22,24,25] is provided in detail in the supplementary material of [21]. The optimisation is run for 30 iterations, which was established to be sufficient through a convergence study. The result of the multi-objective optimisation is a set of solutions that optimally fulfil the two conflicting objectives. The objective function values achieved by the set of optimal solutions create a so called Pareto front, which shows how one objective can be improved at the expense of the other.

2.2. Geometry definition

A set of four basic geometric shapes were used for this study, which are represented in Fig. 2. The parameters that define each geometry are shown in the figure. These represent the optimisation variables that were varied within the optimisation process.

Both upper and lower bounds for each of these optimisation variables were defined, as shown in Table 1. These limits to the hull geometry were defined to avoid the optimisation converging on very large or very small devices. The draft d of all shapes was limited to be no larger than 30 m. This was defined based on the draft used for the floating offshore wind design Pelastar [26], where the purpose is to reduce device oscillations, and so should serve as a limit without constraining the range of possible solutions found through the optimisation process. The length l, beam b and radius r were limited based on the wavelength (λ), which here is taken as the 95% exceedance probability maximum wavelength for each location and is therefore referred to as λ_{MAX}. This ensures that the evaluated devices can be regarded as point-absorbers based on the definition in [10]. The lower bound of 2.5 m was chosen based on [23,27], which was considered a sensible minimum size for a device.

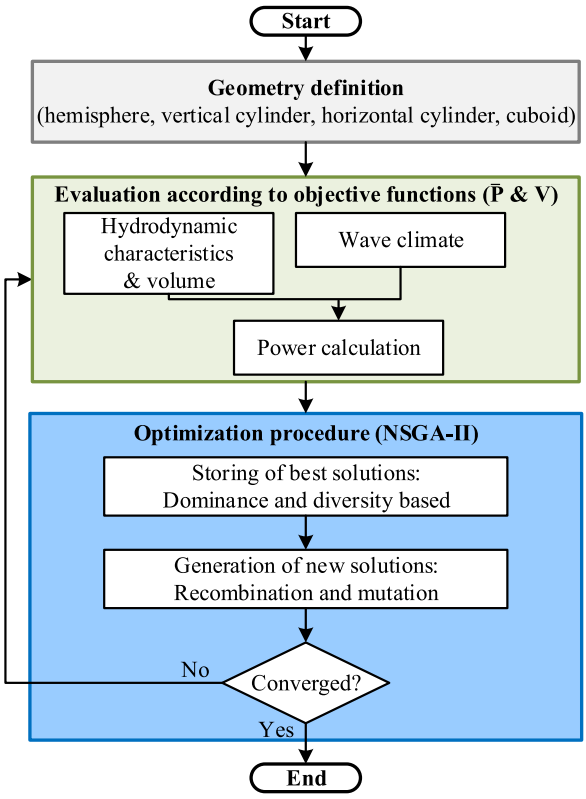

Fig. 1. Flow chart representing the design optimisation process. The considered objective functions here are mean annual produced power $\bar{P}$ and submerged volume V. The used optimisation algorithm is the multi-objective Non-dominated Sorting Genetic Algorithm II (NSGA-II).

Table 1
Bounds used on geometry optimisation variables for each shape. The variables for each shape are defined in Fig. 2 as the radius r, the draft d, the beam b and the width w.

Shape	Bounds
A - Hemisphere	2.5 m $\leq r \leq$ 30 m
B - Vertical cylinder	2.5 m $\leq d \leq$ 30 m, 2.5 m $\leq r \leq \lambda_{MAX}/4$
C - Horizontal cylinder	2.5 m $\leq d \leq$ 30 m, 2.5 m $\leq l \leq \lambda_{MAX}/2$
D - Cuboid	2.5 m $\leq d \leq$ 30 m, 2.5 m $\leq l, b \leq \lambda_{MAX}/2$

2.3. Evaluation according to objective functions

Wave climate

Generic resource scatter diagrams were generated for regions of the North Sea, North Atlantic and Mid Atlantic and for high, medium and low resource levels defined by the annual mean power density, following the method outlined in [28]. These were generated based on resource data in a number of locations within each of those zones, as marked in Fig. 3.

For the purpose of generating fundamental relationships, the two zones with the largest difference in range of occurring periods were used and the best results found at the two zones were selected to generate the final fundamental relationships. This was done so that fundamental relationships could be generated independently from location, but dependent on the resource level. The two locations considered for this purpose were zone C located off the coast of Ireland, and zone F located off the coast of Portugal (see Fig. 3). This provided a total of six scatter diagrams with varying characteristics. The main characteristics associated to the two zones and three resource levels per zone are summarised in Table 2.

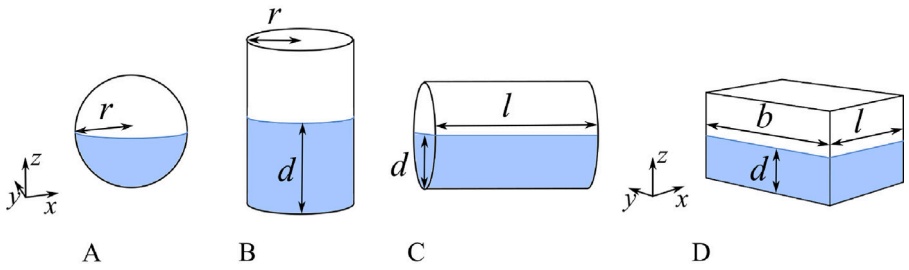

Fig. 2. Basic shapes used in the optimisation process: (A) a hemisphere, (B) a vertical cylinder, (C) a horizontal cylinder and (D) a cuboid (barge/flap). The parameters that define each shape are shown in this figure, namely the radius r, the draft d, the beam b, and the length l. The submerged surface area is represented in blue. The waves are assumed to propagate in the positive x-direction.

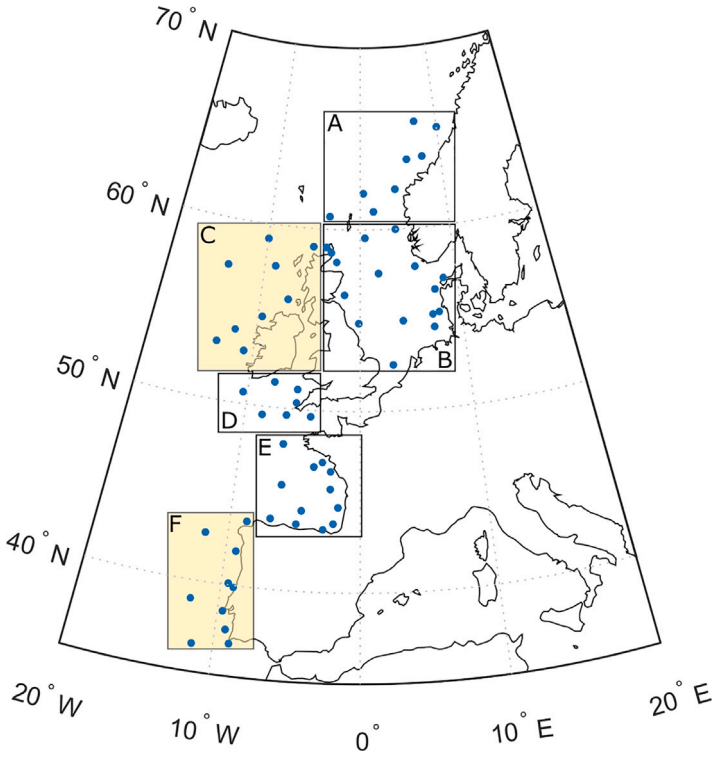

Fig. 3. Map showing the zones of ocean for which corresponding wave climates were considered. The selected and used resource zones are highlighted in yellow.

Table 2
Overview of resource characteristics.

Zone	Resource level	Power density [kW/m]	Water depth [m]	λ_{MAX} [m]
C	Low	15	38	139.44
	Medium	45	115	163.38
	High	75	192	184.72
F	Low	15	38	160.24
	Medium	45	115	206.70
	High	75	192	264.19

Stroke limits

Stroke limits are applied in the calculation of the instantaneous power absorbed by the PTO, by calculating the oscillation time series. If the stroke limit is exceeded, the instantaneous power is set to 0 for that time step. The stroke limits are defined based on the Budal upper bound extension to multiple Degrees of Freedom (DoF) presented by Todalshaug in [10]. The stroke constraint in surge is based on the fact that a restoring moment is required provided by the wave motion, and so the oscillation cannot exceed more than 1/4 of the wavelength λ_{MAX}. For the same reason, the stroke in pitch cannot exceed $\pi/2$. In heave, assuming that the cross-sectional area of the device is constant, then the maximum stroke is defined by the volume of the device, and the waterplane surface area ($V/(2A_w)$). Exceeding this limit would result in the device being out of the water and therefore linked to slamming, or in the device being fully submerged. If we assume that 50% of the device's volume is submerged, for shapes that do not have a constant cross-sectional area, an equivalent approach would be to use the draft of the device as the stroke constraint. Since the total device volume is not defined here, but based on previous projects supported by Wave Energy Scotland a 50% submergence is a representative average of existing devices, the constraint was adapted to be defined as the geometry's draft (d). The PTO stroke limits used here are summarised in Table 3.

Table 3
Assumed stroke limits in the considered modes of motion.

Mode of motion	Stroke limit
Surge	$\pm\lambda_{MAX}/4$
Heave	$\pm d$
Pitch	$\pm\pi/2$

Table 4
Overview of considered case studies. All permutations of the options in this table were evaluated, apart from the combinations including a hemisphere, and a pitching motion.

Shapes	Modes of motion	Zones	Resource levels
A - Hemisphere	Surge	C	Low
B - Vertical cylinder	Heave	F	Medium
C - Horizontal cylinder	Pitch		High
D - Cuboid	Surge & Heave		
	Heave & Pitch		

All generated fundamental relationships should therefore comply with the Budal upper bound and the extension to this limit by Todalshaug.

PTO rating

A preliminary study was performed to understand the effect of applying PTO rating constraints in the power calculation on the results. Constraining the PTO rating results in a cap on the power that can be absorbed with larger volumes. This limit is particularly constraining in the high resource level.

Since the purpose of developing these fundamental relationships is to represent the art-of-the possible, no PTO rating constraints were enforced here to avoid artificially constraining the optimisation space.

Capture width

The maximum capture width limit previously mentioned is considered as an upper bound to the average power produced per sea state following the approach in [23]. Ten realisations of the same sea state are considered and the average power across the ten realisations is employed as the average power produced per sea state. In a given sea state realisation, if the maximum capture width is exceeded then that realisation is discarded. If all ten realisations exceed the maximum capture width, the average power at that sea state is set to zero. All generated fundamental relationships should therefore comply with this limit.

2.4. Summary of cases considered

To define the fundamental relationships, four shapes and three resource levels at two locations were considered. In terms of the considered modes of motion, these include surge, heave, and pitch, and the combinations of surge & heave, and heave & pitch. The reasons for this selection of modes of motion are: (1) Given that uni-directional waves are analysed and all shapes are symmetric to the x-z plane, the rolling and yawing motions were not considered. (2) It was shown in [15,17] that no significant advantage was found in combining surge & pitch or surge & heave & pitch versus the other options considered here, and so these were not included in the current analysis. An overview of all considered cases, which result in 108 permutations is provided in Table 4.

After generating results for the 108 permutations, one fundamental relationship was generated for each resource level by selecting the best shapes at the two considered zones to provide location-independent results for each DoF and shape type. This was done by generating a single Pareto front per resource level by combining the Pareto fronts for the two evaluated zones. An example of this procedure is shown in Fig. 4. A total of 54 fundamental relationships depending on shape, mode of motion and resource level were obtained.

3. Results

As introduced in the previous section, a total of 54 fundamental relationships were generated by considering four shapes, five combinations of modes of motion for power extraction, and three resource levels. To be able to demonstrate the effect of each of these factors, a selection of the results is presented first. This allows to understand and analyse the impacts of these factors independently. Some example relationships as generated with the optimisation process for average produced power to submerged volume are shown in Section 3.1, while all tabulated values can be found in the Supplementary material. Based on these relationships, further relationships are then generated: average produced power to scale in Section 3.2, and both capture width and capture width ratio to scale in Section 3.3. This is done to: (1) gain further insights into the nature of these relationships, and (2) to allow for broader use of these relationships for comparison with state-of-the-art (SOTA) data. To exemplify the use of these fundamental relationships, the 54 resulting relationships in terms of average produced power to scale are then plotted together with state-of-the-art WEC trends to showcase the full range of results and allow for further discussion in Section 4.

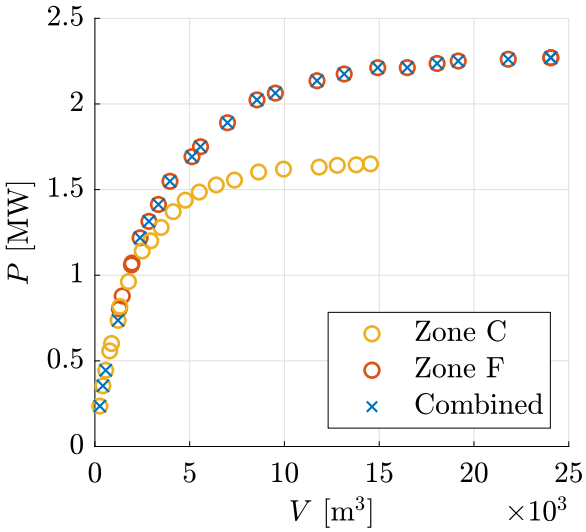

Fig. 4. Example combination of results from two Pareto fronts: one from Zone C and one from Zone F, into one single 'Combined' Pareto front, for the medium resource level for a cuboid oscillating in heave only.

3.1. Relationship of power to volume

The fundamental relationships as generated through the optimisation process are presented in this section. These show how the average produced power varies with submerged volume.

Firstly, the effect of shape on this relationship can be seen in Fig. 5, where the relationship is shown for four shapes and three resource levels, considering surge as an example mode of motion. It can be seen that for all resource levels all shapes perform similarly. However, it can be seen that the hemisphere and the horizontal cylinder show some differences with the vertical cylinder and the cuboid. As shown in [17], when performing WEC geometry optimisation the surface area perpendicular to the mode of motion for power extraction is maximised to maximise power absorption. So in this surging case, the area perpendicular to the surging motion achieved with the horizontal cylinder and the hemisphere will be equivalent. For the same area perpendicular to the surging motion, the overall submerged volume with the horizontal cylinder can be higher than with the hemisphere, and this would explain the relationship achieved with the horizontal cylinder in the medium and higher resource levels extending over higher values of submerged volume. A similar effect can be seen for the vertical cylinder and the cuboid, which can both achieve higher but similar areas perpendicular to the surging motion.

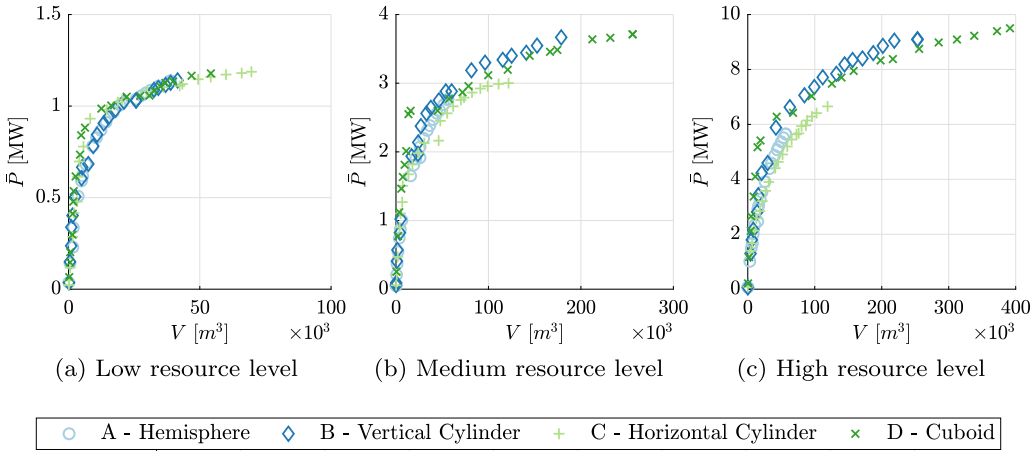

Fig. 5. Optimisation results for the four shapes oscillating in surge only for each of the three resource levels: (a) low, (b) medium and (c) high.

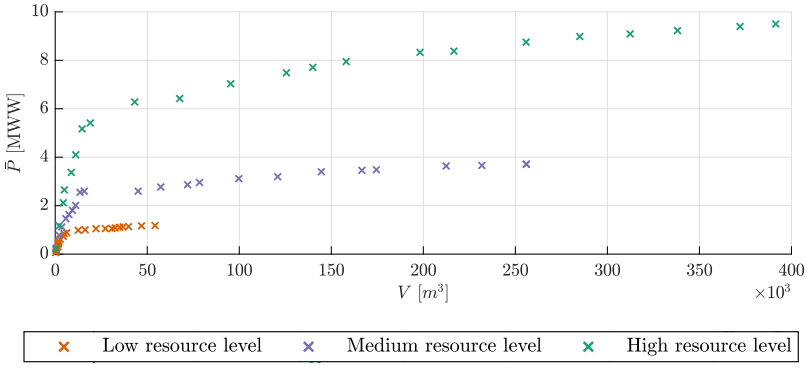

Fig. 6. Optimisation results for a cuboid oscillating in surge only at the three resource levels.

Particularly for the vertical cylinder and the cuboid in surge, a clear limit to increasing power with increasing volume can be seen in Fig. 5. The optimisation results asymptotically approach a limit in average produced power with increasing volume. This would imply that once a minimum dimension is reached (and the area perpendicular to the surging motion is maximised) further increases in volume do not result in significant increases in average power produced. Therefore, for each resource level a maximum submerged volume value can be identified. This is approximately 50,000 m^3 for the low resource level, 200,000 m^3 for the medium resource level, and 350,000 m^3 for the high resource level.

To investigate further the influence of resource available, Fig. 6 shows how power varies with volume for a cuboid absorbing power in surge at the three resource levels. This is a subset of the data in Fig. 5. With limits approaching 1.3, 4, and 10 MW for a resource of 15, 45, and 75 kW/m, respectively; it can be seen this relationship is non-linear.

Secondly, the effect of the employed modes of motion for power extraction on this relationship can be seen in Fig. 7. This shows how power varies with submerged volume for the five modes of motion in the three resource levels, considering a cuboid as an example shape geometry. It can be seen that cuboids absorbing power in heave & pitch have a higher limit to the average absorbed power with a clear advantage versus other combinations of modes of motion with increasing scale. For WECs absorbing power in a single-mode of motion, the pitching motion shows higher power absorption potential across scales, whereas the heaving motion shows a lower power absorption potential and a more limited scale range — with no benefit observed for submerged volumes larger than 40,000 m^3.

3.2. Relationship of power to scale

Rather than relating power to submerged volume an alternative approach is presented, showing the relationship with a representative length scale. This is defined as the cube root of the total volume, assuming the device is 50% submerged. As before, this is shown for all shapes and resource levels for a surging device in Fig. 8, and for all modes of motion and resource levels for a cuboid in Fig. 9.

In general the relationship of average absorbed power to scale when compared to average absorbed power to submerged volume shows a less steep initial increase. Although an asymptotic behaviour with scale increase can still be observed, this is less obvious than in the submerged volume case.

The relationships across shapes and modes of motion remain very similar, but some further details can be observed. On one hand, as it can be seen from Fig. 8 in comparison to Fig. 5 the relationships across shapes remain similar. On the other hand, as it can be seen from Fig. 9 in comparison to Fig. 7 the relationships across modes of motion become more evident. The combination of heave & pitch still shows a higher limit to the average absorbed power at larger scales, but also at lower scales. In the lower scales range, the combination of surge & heave shows a comparable or even better performance in the medium and high resource levels.

All 54 relationships of modes of motion, shape, and resource level are shown in Fig. 10. As previously observed for the cuboid example case, from Fig. 10 it can also be seen for other shapes that devices absorbing power in heave & pitch have a higher limit to the average absorbed power, and this is reached at larger scales, whereas devices absorbing power in surge & heave seem to have potential to achieve higher power absorption at smaller scales. For WECs absorbing power in a single-mode of motion, the pitching motion shows higher

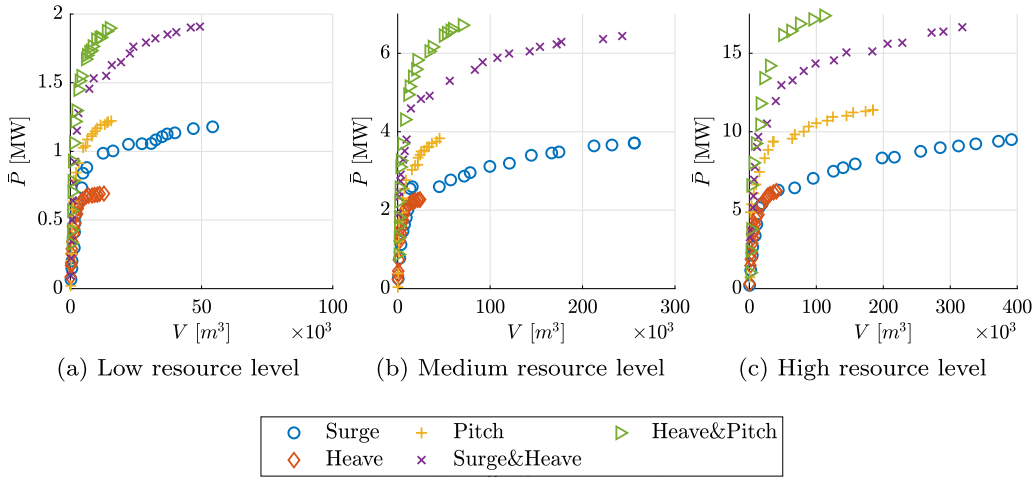

Fig. 7. Optimisation results for the cuboid shape oscillating in all studied combinations of modes of motion for each of the three resource levels: (a) low, (b) medium and (c) high.

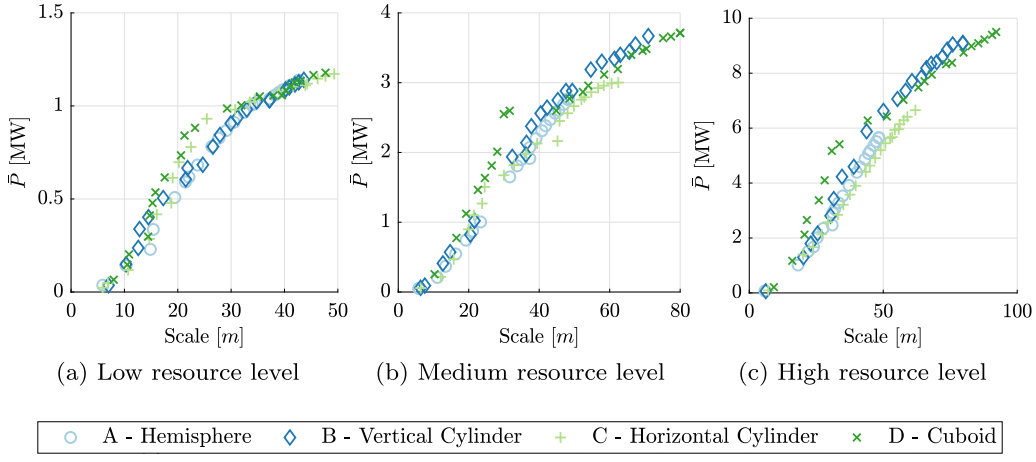

Fig. 8. Optimisation results converted into a relationship of average produced power to scale for the four shapes oscillating in surge only for each of the three resource levels: (a) low, (b) medium and (c) high.

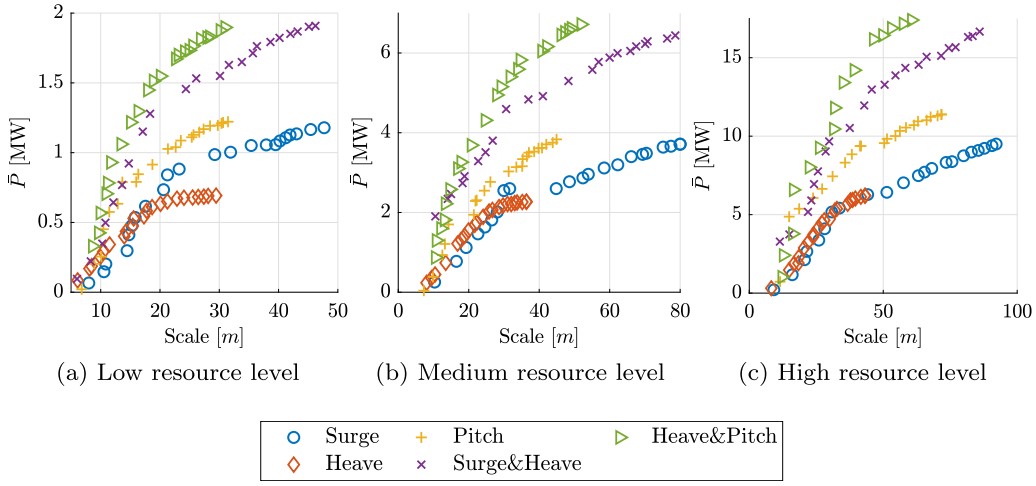

Fig. 9. Optimisation results converted into a relationship of average produced power to scale for the cuboid shape oscillating in all studied combinations of modes of motion for each of the three resource levels: (a) low, (b) medium and (c) high.

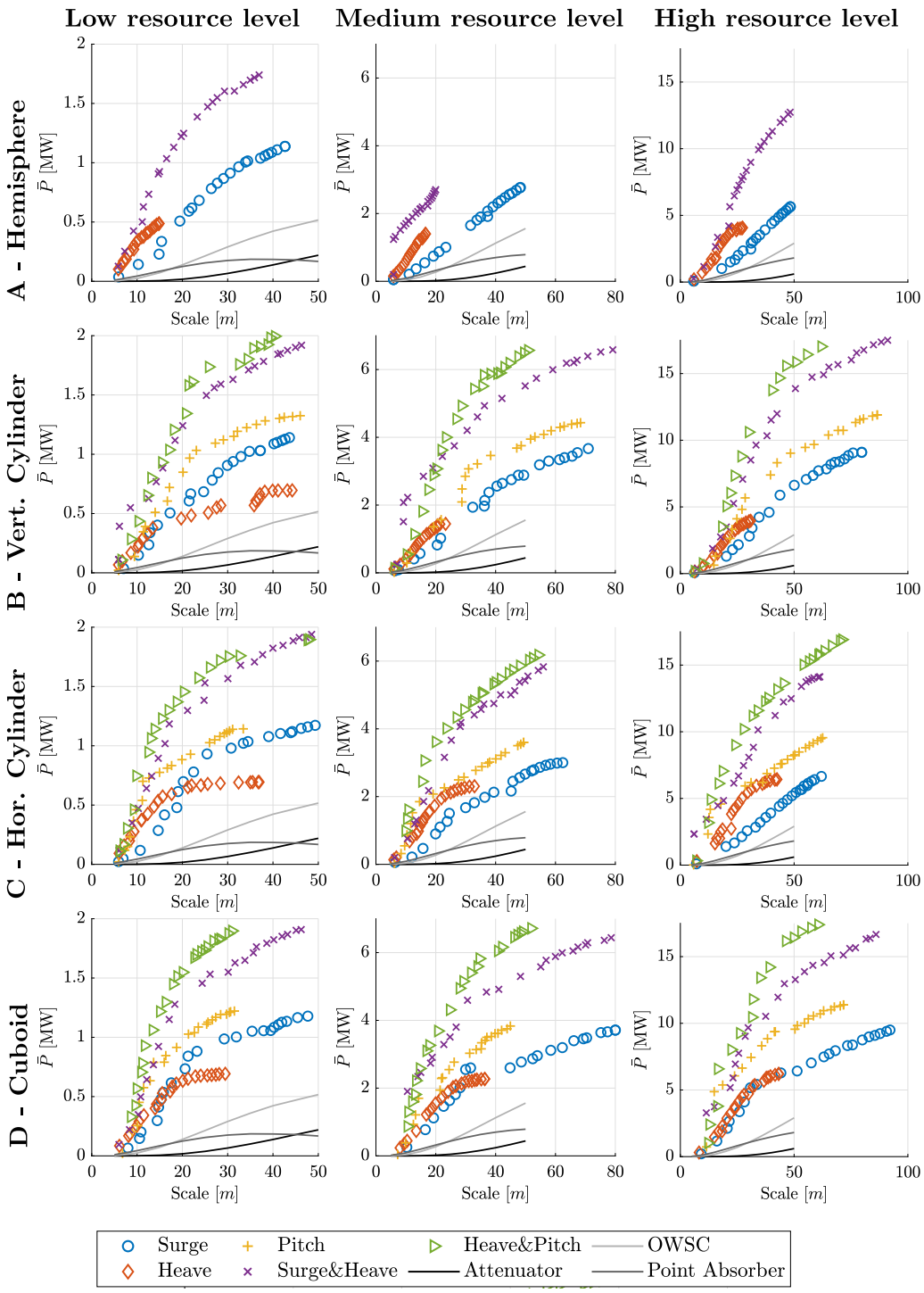

Fig. 10. 54 fundamental relationships in terms of average produced power to scale for four shapes, three resource levels, and five combinations of modes of motion for power extraction. Trends representing the state of the art for three types of wave energy converters are included.

power absorption potential across scales. Heaving-only devices seem to perform well at lower scales, but are consistently outperformed by surging-only and pitching-only devices at larger scales. Across shapes the potential performance per scale is very similar. The hemisphere performs worse than other shapes in the medium and high resource levels, (1) due to the limited modes-of-motion that can be used for power absorption under the assumed conditions, and (2) because in this case the submerged volume and therefore the scale is solely determined by the radius, and so increases scale in this case cannot be tuned to the same extent as with other shapes to benefit the power absorption in a given mode of motion.

3.3. Relationships of capture width and capture width ratio to scale

From the obtained Pareto fronts for the relationships of average absorbed power to submerged volume, the values for the corresponding capture width (CW) and capture width ratio (CWR) were calculated.

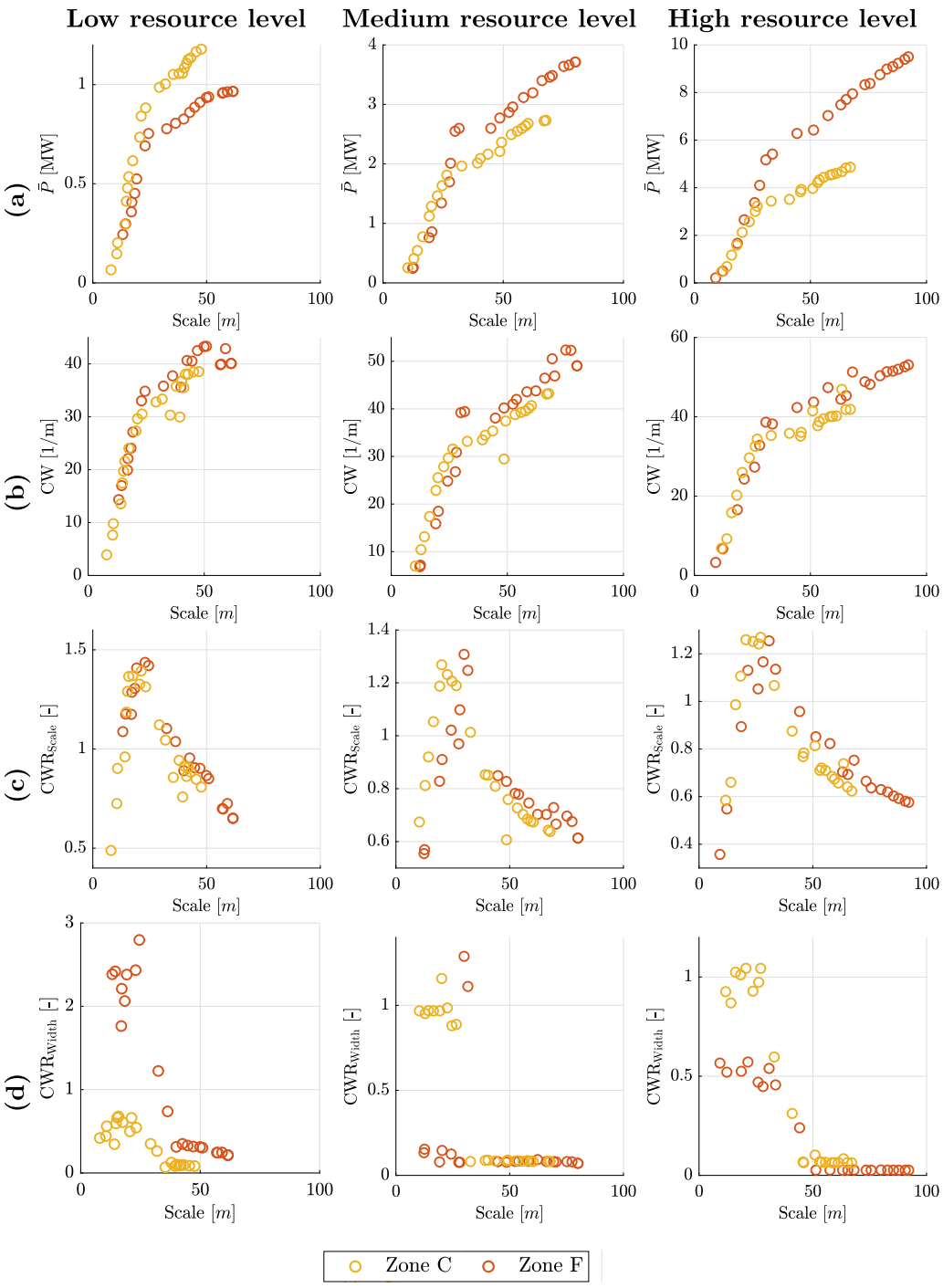

Fig. 11. Optimisation results for $\bar{P}$ to V converted into a relationship of (a) $\bar{P}$ to scale, (b) Capture Width (CW) to scale, (c) Capture Width Ratio based on scale ($\mathrm{CWR_{Scale}}$) to scale, and (d) Capture Width Ratio based on active width ($\mathrm{CWR_{Width}}$) to scale, for a cuboid oscillating in surge only in three resource levels for the two zones. Note that the results are not optimised for these relationships.

For a given sea state CW and CWR were obtained as follows:

$$\mathrm{CW} = \frac{P}{P_{pm}}, \tag{1}$$

where $P_{pm} = \dfrac{\rho g^2 T_e H_{m0}^2}{64\pi}$ for deep water, and

$$\mathrm{CWR} = \frac{P}{P_{pm} B}. \tag{2}$$

Here P is the absorbed power per sea state, P_{pm} is the power per metre crest width available in that sea state, ρ the density of water, g the gravitational acceleration, T_e the energy period, H_{m0} the significant wave height, and B the characteristic length of the device. Here CWR has been calculated using two different measures for B, $\mathrm{CWR_{Width}}$ uses the active width of the device as employed by Babarit in [12], whereas for $\mathrm{CWR_{Scale}}$, B is assumed to be equivalent to the device scale.

Overall, this means CW is an indicator for conversion efficiency if considering power absorption only, whereas CWR indicates conversion efficiency relative to device scale.

Example relationships of average CW and CWR to scale are shown in Fig. 11 for a cuboid oscillating in surge and in Fig. 12 for a hemisphere oscillating in heave. Because these parameters are dependent on the available resource through P_{pm}, they are location specific, and

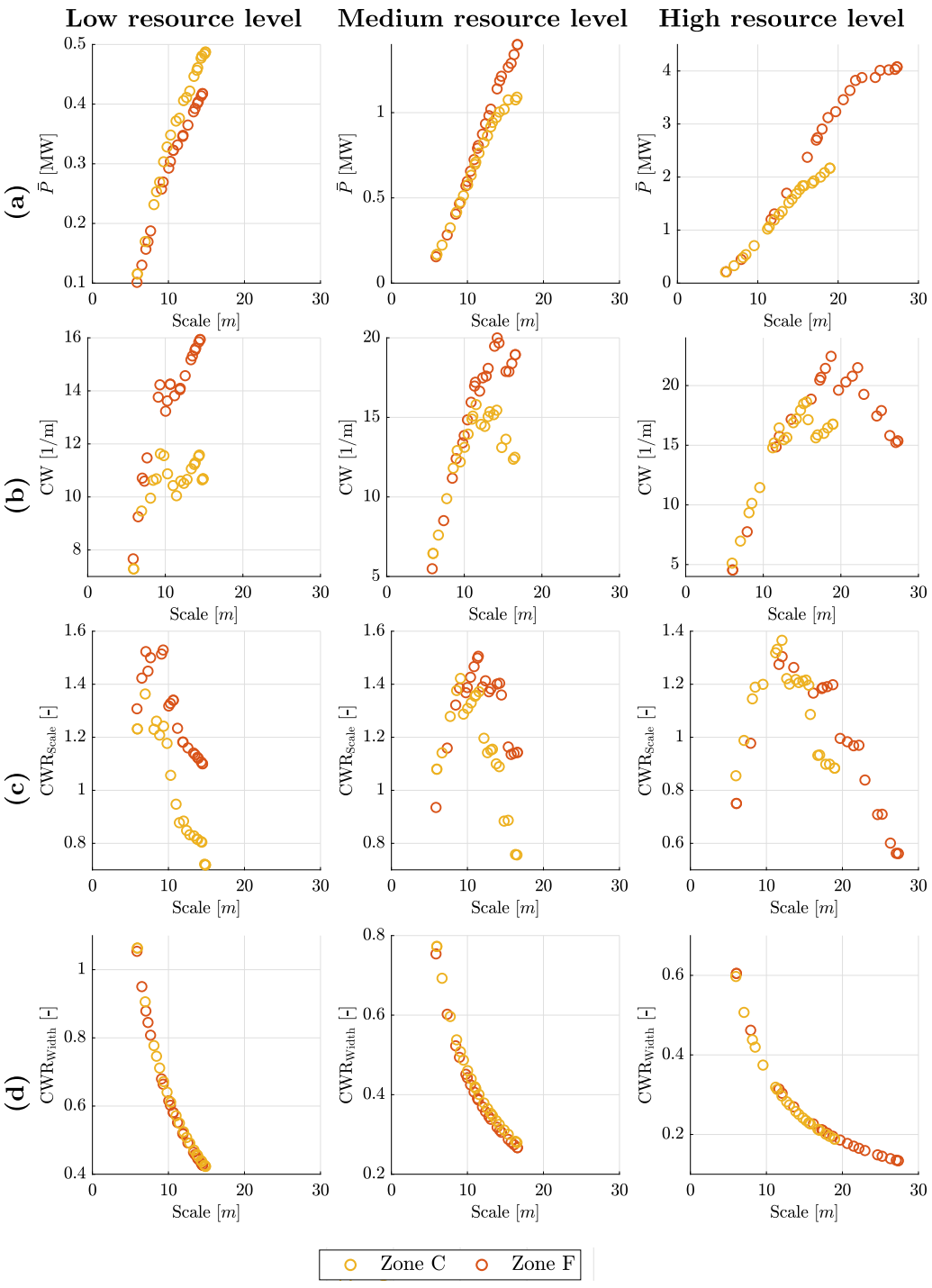

Fig. 12. Optimisation results for $\bar{P}$ to V converted into a relationship of (a) $\bar{P}$ to scale, (b) Capture Width (CW) to scale, (c) Capture Width Ratio based on scale ($\mathrm{CWR_{Scale}}$) to scale, and (d) Capture Width Ratio based on active width ($\mathrm{CWR_{Width}}$) to scale, for a hemisphere oscillating in heave only in three resource levels for the two zones. Note that the results are not optimised for these relationships.

so they are shown for the two zones separately. To obtain a location independent relationship, as before, the best results (highest CW and CWR values per scale) between the two sites could be taken to be representative of the achievable limit. It should be noted however, that the results shown here, do not represent solutions optimised to maximise CW or CWR and scale, but solutions found to maximise average absorbed power and submerged volume.

In both cases and across resource levels, peaks in CW and CWR per scale can be identified, with the highest CW reached at higher scales than CWR. That is, the peak in performance is achieved at higher scales if looking for maximum conversion efficiency only, than if looking at it relative to device scale or active width.

This existence of an optimal scale is more evident when looking at CWR than at CW. That is, in the case of the surging cuboid CW keeps increasing with scale and so a peak is not so clearly identifiable. However, in the case of the heaving hemisphere a peak between 10 and 15 m scale can be identified depending on the resource level — with higher scales being more suitable for higher resource levels.

If looking at $\mathrm{CWR_{Scale}}$ peaks can be identified in both cases, where it can be seen that the peak also takes place at higher scales with

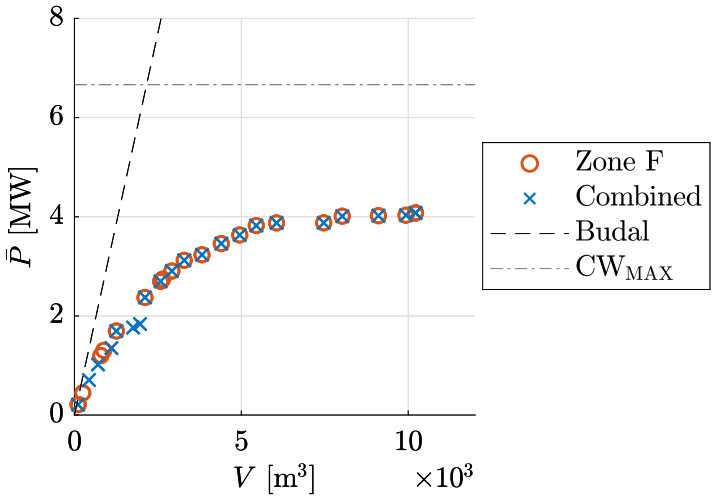

Fig. 13. Results from Pareto fronts for Zone F and single 'Combined' Pareto front including results from both Zone F and Zone C - representing the generated fundamental relationship for the high resource level for a hemisphere oscillating in heave only, in comparison with the existing physical limits calculated for Zone F.

increasing resource level. Optimal scales for the cuboid in low, medium, and high resource levels were respectively found at 15–19 m, 20–30 m, and 21 m, and for the heaving hemisphere at 7 m, 9 m, and 9–12 m.

CWR_{Width} shows a more Pareto-front-like shape, particularly in the heaving hemisphere case, where an increase in CWR_{Width} is observed with decreasing scale.

This different behaviour of the CWR_{Scale} and CWR_{Width} seems to indicate that an optimal scale may exist to achieve maximum CWR_{Scale} for a given location, hull shape and mode-of-motion for power extraction, whereas to achieve the maximum CWR_{Width} the 'optimal' solution is the one with the smallest width. This would indicate that in the obtained solutions scale or submerged volume are a better indicator to guide design decisions than the active width, or the commonly used measure of CWR_{Width}.

4. Discussion

4.1. How do the generated fundamental relationships compare to existing physical limits?

The generated fundamental relationships can be found within the bounds defined through the existing physical limits. The commonly represented example of a heaving sphere is shown in Fig. 13, where the physical limits are calculated for Zone F resource data, and the results are provided in comparison to, both, the optimisation results obtained for Zone F and for the two zones combined into a final fundamental relationship. The existing physical limits are generally shown in terms of produced power per wave period. However, in this case to allow for comparison the average power when accounting for sea state occurrence probability is shown for the existing physical limits — where power per sea state was calculated at the energy period. The Budal upper bound is defined to be valid for small volumes. This also becomes evident from Fig. 13, where the Budal upper bound, linking the average produced power to device size behaves similarly to the found fundamental relationships for smaller volumes. However, the Budal upper bound keeps quickly increasing with increasing volume surpassing the maximum capture width limit.

This shows that the produced fundamental relationships are able to provide realistic limits by considering geometry and resource characteristics.

4.2. How do the generated fundamental relationships compare to state-of-the-art WECs?

To demonstrate state-of-the-art (SOTA) WECs compared to the generated fundamental relationships for possible power, trends for three types of WECs: oscillating wave surge converters (OWSCs), point absorbers, and attenuators were generated as seen in Fig. 10. These trends are based on various sources including numerical models from the National Renewable Energy Lab (NREL) [29], and tank test and open water test data from both the Oyster Aquamarine Power project and the Wave Energy Scotland Programme [28,30,31].

Of the WECs considered, only data from 13 WECs fell into the categories of OWSCs, point absorbers or attenuators, which were used to create the SOTA trends, so to be comparable with the fundamental relationships.

The method used to find the SOTA relationships started with the power matrices, using interpolation between sea states to complete power matrices with any missing data. The active width of each of the cases was defined using the hull scale and the power matrices were scaled to different active widths from 5 m to 50 m in 5 m steps using Froude scaling. Annual mean power was calculated for each case by taking the product sum of the power matrices and the same resource matrices that were used in the creation of the fundamental relationships. Results for the same WEC types were then averaged. This allowed the generalised SOTA relationship between scale and power to be defined for each of the three resource levels. This method is outlined fully in [14].

As it can be seen from Fig. 10 SOTA WEC's performance is lower than the fundamental relationships in all cases. For example, if comparing the SOTA OWSC with a surging cuboid, at a 25 m scale the SOTA average produced power is approximately 1/4 of the fundamental relationship limit. According to the fundamental relationships, an average power absorption of 0.5 MW can be reached at a scale of 15 m, whereas the SOTA WECs would only achieve this value at a 50 m scale. This result is both expected and verifies the work presented here. The fundamental relationships are developed to demonstrate what is theoretically possible, and so it is expected that the current SOTA in wave energy has never met these limits. This is also evidence that the generated limits are in the range expected and that they can be used to identify potential areas for innovation.

5. Conclusions

A multi-objective optimisation approach was employed to generate fundamental relationships between average absorbed power and submerged volume for wave energy converters. Four shapes, absorbing power in five combinations of modes of motion, in three different resource levels were evaluated to produce a total of 54 relationships.

Relationships were presented in terms of average absorbed power to submerged volume, and average absorbed power to scale. A limit in the average produced power with increasing size was observed across resource levels, shapes and modes of motions. Devices absorbing power in heave & pitch showed a higher limit to the average absorbed power, which was reached at larger scales. Devices absorbing power in surge & heave demonstrated potential to achieve higher power absorption at smaller scales. For devices absorbing power in a single-mode of motion, those utilising the pitching motion showed higher power absorption potential across scales. Further relationships between capture width and capture width ratio were derived based on the optimal Pareto fronts of average absorbed power and submerged volume, which showed that optimal scale values can be identified to achieve maximum CW and CWR, respectively.

The limits were compared with existing physical limits defined through the maximum capture width and the Budal upper bound, as well as with state-of-the-art wave energy converters. The generated relationships were lower than the existing physical limits and higher than the extrapolated performance of state-of-the-art WECs in all cases. The fact that the generated relationships can be obtained for different shapes, and accounting for more detailed resource characteristics than with previous limits, while representing optimal power absorption cases, translates in more realistic design limits that developers can use as reference to compare their devices to. This can help developers and funding bodies better understand the relative performance of a real device, and which parameters of that device may need to be exploited further to improve performance. Particularly if used in the context of structured innovation processes such as facilitated with the scenario creation or the structured innovation tools developed within the DTOceanPlus project, they can support the identification of areas for disruptive innovation.

The method presented here can also be exploited to generate further fundamental relationships in the future, not only by exploring other locations or shapes, but also by exploring different combinations of conflicting objectives. The added advantage of developing such a flexible method for the definition of fundamental relationships is that other types of fundamental relationships e.g. linking power performance and reliability can be derived (see, for example, [32]), or combined with other existing relationships. For example, a relationship between the cost and the scale of wave energy converters was derived in [14]. Through the fundamental relationship derived here between average produced power and scale, a new fundamental relationship could then be obtained between cost and average produced power.

CRediT authorship contribution statement

Anna Garcia-Teruel: Conceptualization, Methodology, Software, Formal analysis, Visualization, Writing – original draft. **Owain Roberts:** Conceptualization, Methodology, Resources, Visualization, Writing – review & editing. **Donald R. Noble:** Conceptualization, Writing – review & editing. **Jillian Catherine Henderson:** Conceptualization, Resources, Writing – review & editing. **Henry Jeffrey:** Funding acquisition.

Declaration of competing interest

The authors declare that they have no known competing financial interests or personal relationships that could have appeared to influence the work reported in this paper.

Acknowledgements

The authors want to acknowledge Dr. Ines Tunga for the helpful discussions and feedback. This publication has been supported by the H2020 project DTOceanPlus (Advanced Design Tools for Ocean Energy Systems Innovation, Development and Deployment). The project has received funding from the European Union's Horizon 2020 research and innovation programme under grant agreement No 785921. For the purpose of open access, the author has applied a Creative Commons Attribution (CC BY) licence to any Author Accepted Manuscript version arising from this submission.

Appendix A. Supplementary data

Supplementary material related to this article can be found online at https://doi.org/10.1016/j.renene.2022.09.053.

References

[1] European Commission, European Commission : CORDIS : Projects and results : Home, 2020, https://cordis.europa.eu/projects/en, (Accessed on 04/12/2020).
[2] R. Kohli, J. Fishman, M. Hyatt, Decision gate process for assessment of a technology development portfolio, 2012, http://dx.doi.org/10.2514/6.2012-5182C.
[3] R. Costello, K. Nielsen, J. Weber, N. Tom, J.D. Roberts, WaveSPARC: Evaluation of innovation techniques for wave energy, in: Proc of the 13th European Wave and Tidal Energy Conference, 2019, URL https://www.osti.gov/biblio/1641798.
[4] P. Kerr, D.R. Noble, J. Hodges, H. Jeffrey, Implementing radical innovation in renewable energy experience curves, Energies 14 (9) (2021) http://dx.doi.org/10.3390/en14092364.
[5] Wave Energy Scotland, Wave Energy Scotland- Driving the development of wave energy technology in Scotland, 2021, Accessed: 07/05/2021. URL https://www.waveenergyscotland.co.uk/.
[6] Department of Energy, About the wave energy prize, 2021, accessed: 09/07/2021. URL https://www.energy.gov/eere/water/about-wave-energy-prize.
[7] J. Falnes, A review of wave-energy extraction, Mar. Struct. 20 (4) (2007) 185–201, http://dx.doi.org/10.1016/j.marstruc.2007.09.001.
[8] J.N. Newman, Marine Hydrodynamics, The Massachusetts Institute of Technology, 1977.
[9] J. Falnes, Ocean Waves and Oscillating Systems, Cambridge University Press, New York, 2002.
[10] J.H. Todalshaug, Practical limits to the power that can be captured from ocean waves by oscillating bodies, Int. J. Mar. Energy 3–4 (2013) http://dx.doi.org/10.1016/j.ijome.2013.11.012.
[11] N.M. Tom, Revisiting theoretical limits for one degree-of-freedom wave energy converters, J. Energy Resour. Technol. Trans. ASME 143 (9) (2021) 1–9, http://dx.doi.org/10.1115/1.4049287.
[12] A. Babarit, A database of capture width ratio of wave energy converters, Renew. Energy 80 (2015) 610–628, http://dx.doi.org/10.1016/j.renene.2015.02.049.
[13] I. Tunga, A. Garcia-Teruel, D.R. Noble, J. Henderson, Addressing European ocean energy challenge: The DTOceanPlus structured innovation tool for concept creation and selection , Energies 14 (2021) http://dx.doi.org/10.3390/en14185988.
[14] O. Roberts, J.C. Henderson, A. Garcia-Teruel, D.R. Noble, H. Jeffrey, Bringing structure to the wave energy innovation process with the development of a techno-economic tool, Energies 14 (2021) http://dx.doi.org/10.3390/en14248201.
[15] A. Garcia-Teruel, Geometry Optimisation of Wave Energy Converters (Ph.D. thesis), The University of Edinburgh, 2020, http://dx.doi.org/10.7488/era/213.
[16] MIT, WAMIT user manual, 2016, (Accessed: 10/02/2016). URL http://www.wamit.com/manualupdate/V70_manual.pdf.
[17] A. Garcia-Teruel, D.I.M. Forehand, Optimal wave energy converter geometry for different modes of motion, in: Advances in Renewable Energies Offshore: Proceedings of the 3rd International Conference on Renewable Energies Offshore (RENEW 2018), Lisbon, 2018, pp. 299–305.
[18] A. Garcia-Teruel, D.I.M. Forehand, A review of geometry optimisation of wave energy converters, Renew. Sustain. Energy Rev. (2021) http://dx.doi.org/10.1016/j.rser.2020.110593.
[19] K. Deb, S. Agrawal, A. Pratap, T. Meyarivan, A fast elitist non-dominated sorting genetic algorithm for multi-objective optimization: NSGA-II, in: Proc. of the 6th International Conference on Parallel Problem Solving from Nature (PPSN VI), Springer-Verlag, London, 2000.
[20] S. Baskar, S. Tamilselvi, P. Varshini, MATLAB code for constrained NSGA II, 2015, URL https://uk.mathworks.com/matlabcentral/fileexchange/49806-matlab-code-for-constrained-nsga-ii-dr-s-baskar-s-tamilselvi-and-p-r-varshini.

[21] A. Garcia-Teruel, B. DuPont, D.I.M. Forehand, Hull geometry optimisation of wave energy converters: On the choice of the objective function and the optimisation formulation, Appl. Energy 298 (2021) http://dx.doi.org/10.1016/j.apenergy.2021.117153.

[22] H. Mühlenbein, D. Schlierkamp-Voosen, Predictive models for the breeder genetic algorithm, Evol. Comput. 1 (1) (1993) 25–49, http://dx.doi.org/10.1162/evco.1993.1.1.25.

[23] A. McCabe, Constrained optimization of the shape of a wave energy collector by genetic algorithm, Renew. Energy 51 (2013) 274–284, http://dx.doi.org/10.1016/j.renene.2012.09.054.

[24] K. Deb, D. Kalyanmoy, Multi-Objective Optimization using Evolutionary Algorithms, John Wiley & Sons, 2001, p. 497, URL http://dl.acm.org/citation.cfm?id=559152.

[25] K. Deb, S. Pratab, S. Agarwal, T. Meyarivan, A fast and elitist multiobjective genetic algorithm: NGSA-II, IEEE Trans. Evol. Comput. 6 (2) (2002) 182–197, http://dx.doi.org/10.1109/4235.996017.

[26] W.L. Hurley, C.P. Nordstrom, PelaStar Cost of Energy : A Cost Study of the PelaStar Floating Foundation System in UK Waters, Tech. rep., Glosten, 2014.

[27] A. Garcia-Teruel, B. DuPont, D.I.M. Forehand, Hull geometry optimisation of wave energy converters: On the choice of the optimisation algorithm and the geometry definition, Appl. Energy 280 (2020) http://dx.doi.org/10.1016/j.apenergy.2020.115952.

[28] O. Roberts, Structured Innovation Approach for Application to the Wave Energy Sector (Ph.D. thesis), The Univesity of Edinburgh, 2020, http://dx.doi.org/10.7488/era/615.

[29] NREL, Reference Model 5 (RM5): Oscillating Surge Wave Energy Converter, Tech. rep., 2015.

[30] P. Ricci, J. Lopez, I. Touzon, O. Duperray, J.L. Villate, A methodology for the global evaluation of wave energy array performance, in: Proc. of the 4th International Conference on Ocean Energy, 2012.

[31] D. Dunnett, J. Wallace, Electricity generation from wave power in Canada, Renew. Energy (2009) http://dx.doi.org/10.1016/j.renene.2008.04.034.

[32] A. Garcia-Teruel, C.E. Clark, Reliability-based hull geometry optimisation of a point-absorber wave energy converter with power take-off structural reliability objectives, IET Renewable Power Generation 15 (14) (2021) 3255–3268, http://dx.doi.org/10.1049/rpg2.12249.